

# Molecular Origin of the Asymmetric Photoluminescence Spectra of CsPbBr<sub>3</sub> at Low Temperature

Ariadni Boziki, M. Ibrahim Dar, Gwénoél Jacopin, Michael Grätzel, and Ursula Rothlisberger\*

Cite This: *J. Phys. Chem. Lett.* 2021, 12, 2699–2704

Read Online

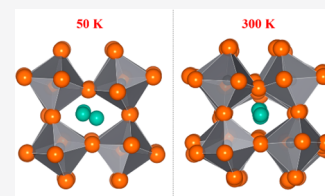
ACCESS |

Metrics & More

Article Recommendations

Supporting Information

**ABSTRACT:** CsPbBr<sub>3</sub> has received wide attention due to its superior emission yield and better thermal stability compared to other organic–inorganic lead halide perovskites. In this study, through an interplay of theory and experiments, we investigate the molecular origin of the asymmetric low-temperature photoluminescence spectra of CsPbBr<sub>3</sub>. We conclude that the origin of this phenomenon lies in a local dipole moment (and the induced Stark effect) due to the preferential localization of Cs<sup>+</sup> in either of two off-center positions of the empty space between the surrounding PbBr<sub>6</sub> octahedra. With increasing temperature, Cs<sup>+</sup> ions are gradually occupying positions closer and closer to the center of the cavities. The gradual loss of ordering in the Cs<sup>+</sup> position with increasing temperature is the driving force for the formation of tetragonal-like arrangements within the orthorhombic lattice.



Hybrid organic–inorganic lead halide perovskites have received much attention due to their broad spectrum of applications as promising materials for solar cells,<sup>1–4</sup> light-emitting diodes (LEDs),<sup>5,6</sup> lasers,<sup>7,8</sup> resistive-switching memories,<sup>9,10</sup> X-ray image detectors,<sup>11,12</sup> and piezoelectric energy generators.<sup>13</sup> Among the different halide perovskite compounds, CsPbBr<sub>3</sub> is particularly promising due to its superior emission yield and better thermal stability compared to other organic–inorganic lead halide perovskites.<sup>14–16</sup> Currently, a variety of LED devices and optically pumped lasing systems based on CsPbBr<sub>3</sub> have been realized.<sup>8,17,18</sup> However, despite the rapid progress in material synthesis and device fabrication, the understanding of the fundamental properties of CsPbBr<sub>3</sub> is still evolving.<sup>16,19,20</sup> For a full realization of its potential for several technological applications, it is important to gain further insight into the interplay of the photophysical processes and the structural characteristics of CsPbBr<sub>3</sub>.

Indeed, many of the properties of CsPbBr<sub>3</sub> have been known for over 60 years.<sup>21</sup> It is well-known that CsPbBr<sub>3</sub> undergoes two phase transitions, one at 361 K from an orthorhombic to a tetragonal phase and a second one at 403 K from the tetragonal to a cubic phase.<sup>22</sup> In addition to this, absorption spectroscopy suggests that the compound is a direct semiconductor with a band gap that lies within the range of 2.25–2.36 eV, as reported by different groups.<sup>16,23</sup> The exploration of the emission characteristics, across a wide temperature range, can provide important information regarding the performance of solar cells and LED devices under realistic conditions. Previous studies have reported that temperature-dependent photoluminescence (PL) measurements for MAPbI<sub>3</sub> and MAPbBr<sub>3</sub> exhibit a double emission peak at low temperatures.<sup>24–26</sup> The two PL peaks are associated with MA-ordered and MA-disordered orthorhombic domains with different emission characteristics due to the presence/absence

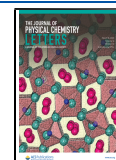
of a Stark effect induced by the dipolar field of the organic cations.<sup>24</sup> However, for CsPbBr<sub>3</sub>, the monovalent cation does not possess a permanent dipole moment, and there seems to exist a disagreement between experimental results concerning the presence and, respectively, absence of a double emission peak.<sup>16,27–29</sup> Stoumpos et al.<sup>16</sup> reported that, in PL measurements at 46 K, two emission peaks are observed at 2.29 and 2.31 eV. Similarly, Lee et al.<sup>29</sup> observed an asymmetry of the PL spectra of CsPbBr<sub>3</sub> quantum dots for temperatures lower than 250 K, which was attributed to a side-peak emission that is located at a lower energy than the band-edge peak. On the one hand, the authors rationalized this anomalous splitting of the emission peak at temperatures less than 250 K with a phase transition of the crystal structure. On the other hand, Han et al.<sup>27</sup> performed temperature-dependent PL measurements for CsPbBr<sub>3</sub> nanocrystals in the temperature range of 80–270 K and observed a spectral band that is approximately symmetric with no obvious double emission peak.

Here, we approach this issue from a combined theoretical and experimental perspective. With the help of first-principles molecular dynamics (MD) simulations and temperature-dependent PL experiments, we investigate the PL spectra of CsPbBr<sub>3</sub> at low temperatures. Our first-principles MD simulations show that, at low temperature, the Cs<sup>+</sup> cations occupy asymmetric positions that are gradually shifted to the center of the cavities with increasing temperature, in agreement

Received: January 25, 2021

Accepted: February 26, 2021

Published: March 11, 2021



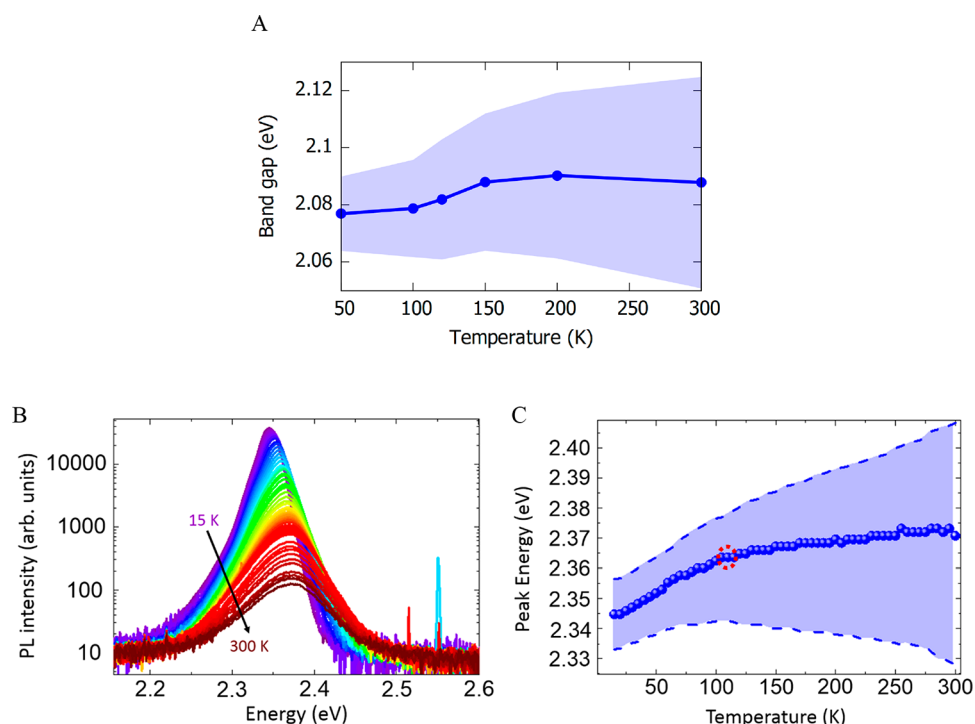


**Figure 1.** Temperature-dependent band gap and emission characteristics of CsPbBr<sub>3</sub>. (A) Thermal evolution of the average Kohn–Sham band gap of CsPbBr<sub>3</sub> from ab initio MD simulations. The light blue shaded area corresponds to the standard deviation. (B) Temperature-dependent PL spectra of CsPbBr<sub>3</sub>. The transition from purple to brown color corresponds to an increase of temperature from 15 to 300 K. (C) The shift of the maximum of the PL bands as a function of temperature. The red circle indicates the region where the change of slope occurs.

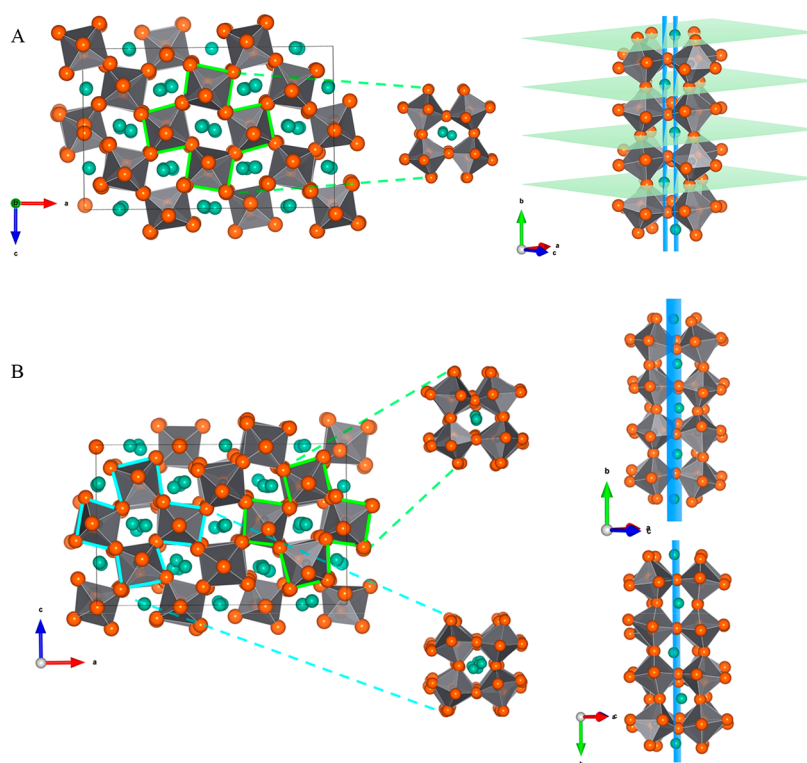


**Figure 2.** Local structures from ab initio MD simulations. At the left-hand side, snapshots of the simulation box are shown, where specific areas are selected and projected, by orienting the *a*-, *b*-, and *c*-axes differently, (shown on the right-hand side). Cs<sup>+</sup> (green balls), Br<sup>-</sup> (orange balls), Pb<sup>2+</sup> (silver balls). (A) Local structure of the 50 K trajectory. The position of Cs<sup>+</sup> in the empty space between the octahedra has a characteristic pattern, where each Cs<sup>+</sup> that belongs to a specific layer (light green layers shown at the right-hand side of the figure) is shifted toward the opposite direction of the Cs<sup>+</sup> that belongs to the next neighboring (light blue) layer, creating two distinct layers (light blue) of Cs<sup>+</sup>. (B) Local structure of the 300 K trajectory. Cs<sup>+</sup> are occupying positions that are more and more near to the center of the cavities.

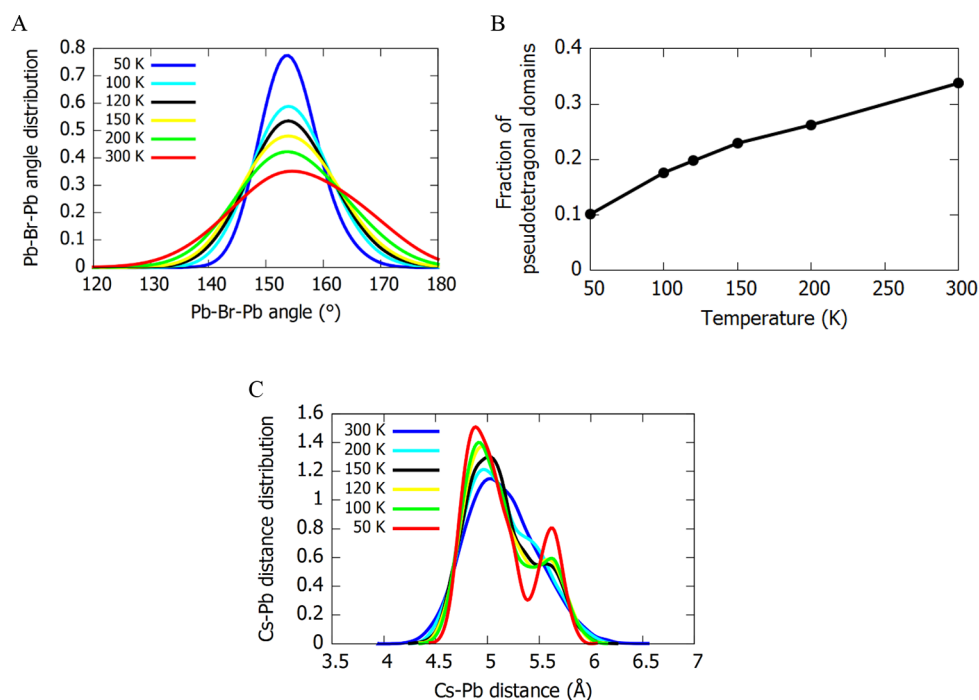


**Figure 3.** Analysis of molecular dynamics trajectories. (A) Thermal evolution of the Pb–Br–Pb angle distribution. The data were fitted by employing Gaussian functions. (B) Fraction of pseudotetragonal domains in the orthorhombic structure of CsPbBr<sub>3</sub> as a function of temperature. (C) Thermal evolution of the nearest Cs–Pb distance distribution. The data were fitted to Gaussian functions.

with the gradual loss of asymmetry observed in the experimental PL spectra as a function of temperature. Our investigation thus provides new insights into the interplay between the photophysical processes and the structural characteristics of CsPbBr<sub>3</sub> at temperatures below the first phase transition (<361 K).<sup>22</sup>

We performed ab initio MD simulations within the Car–Parrinello MD scheme,<sup>30</sup> employing the NVT ensemble for a range of different temperatures (50, 100, 120, 150, 200, and 300 K) using a real-space super cell of 240 atoms. The band gap of this real-space cell at 0 K is 2.07 eV, that is, slightly reduced compared to the fully k-point converged value of 2.14 eV. Equilibrated trajectories of ~4 ps for temperatures at 50, 100, 120, 150, and 200 K as well as an equilibrated trajectory of 12 ps at 300 K were produced. The analysis of these trajectories allows us to determine the finite-temperature band gap of CsPbBr<sub>3</sub> by calculating the maximum of the peak and the standard deviation of the thermal distribution at each temperature.

As shown in Figure 1A, the band gap increases as a function of temperature. This behavior of lead-halide perovskites is well-known<sup>24</sup> and is due to the decrease in the antibonding orbital overlap of the divalent cations and anions due to thermal fluctuations but at variance to the behavior of classical Varshni semiconductors. In addition, the band gap does not increase as a linear function of temperature as shown in Figure 1A. In fact, the variation of the band gap as a function of temperature can roughly be divided into two regimes with a change of slope, which takes place around a temperature range of 100–150 K. This change in slope is similar to the case of MAPbI<sub>3</sub> and could thus be associated with two different microscopic environments. To confirm such a hypothesis, we also performed temperature-dependent time-integrated PL measurements in CsPbBr<sub>3</sub> film samples.<sup>31</sup> The temperature-dependent emission shown in Figure 1B shows an asymmetric peak at low

temperatures (<180 K), which becomes more symmetric with increasing temperature. To compare the finite-temperature band gap that we calculated by performing MD simulations with experimental values, we plotted the shift of the maximum of the PL spectra as a function of temperature (Figure 1C). Indeed, as predicted by the calculations, a change of slope at ~120 K is observed.

Dual-emission behavior has been observed for MA<sup>+</sup>-based halide perovskites where it is attributed as mentioned above to MA<sup>+</sup> disordered orthorhombic domains with different emission characteristics due to the presence/absence of a Stark effect induced by the dipolar field of the organic cations.<sup>24</sup> However, in the case of purely inorganic CsPbBr<sub>3</sub>, it is not obvious what the molecular origin could be. For this reason, we analyzed the data from the first-principles MD simulations to identify the structural characteristics of CsPbBr<sub>3</sub> at different temperatures.

In Figure 2, two local structures extracted from the trajectories at 50 and 300 K, respectively, are shown. We observe that, at 50 K (Figure 2A), the Cs<sup>+</sup> ions show a particular pattern when occupying the empty space between the octahedra. This pattern can be described by two different alternating layers, each of them consisting of a series of horizontally aligned Cs<sup>+</sup> occupying either of the two off-center positions as shown in the right-hand side of Figure 2A. This effect is a consequence of the relatively small size of the Cs<sup>+</sup> ion that only occupies part of the available interoctahedral space and is obvious only when looking along one direction of the orthorhombic lattice. By observing the lattice from the other two directions, Cs<sup>+</sup> are forming only one layer, their position being near to the center of the empty space between the octahedra. At higher temperatures this ordered behavior vanishes, and at 300 K, Cs<sup>+</sup> are occupying positions near the center of the cavities with respect to all three lattice directions (Figure 2B).

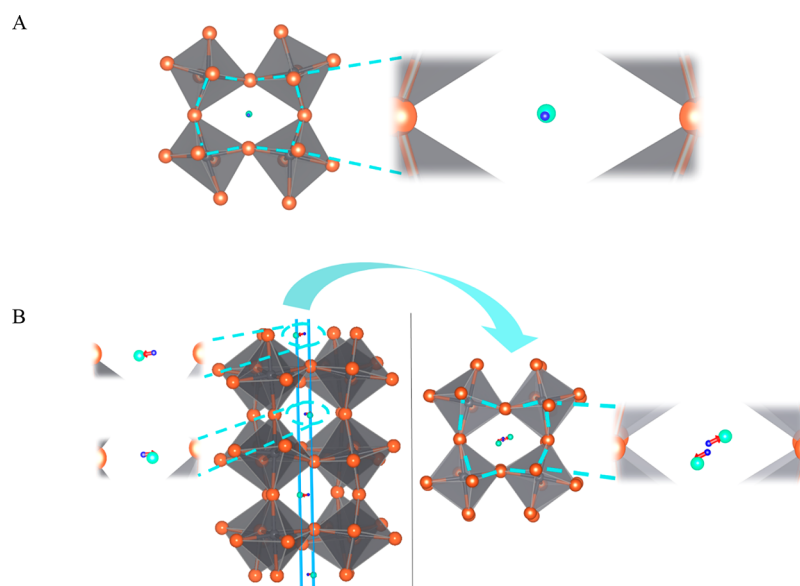


**Figure 4.** Local dipoles. Local structures of the ab initio MD trajectories, where the empty space between the octahedra is selected and projected. Cs<sup>+</sup> (green balls), Br<sup>-</sup> (orange balls), Pb<sup>2+</sup> (silver balls). (A) Local structure of the 300 K trajectory. No dipole moment is observed since Cs<sup>+</sup> assumes positions more and more near the center of cavity (blue ball). (B) Local structure of the 50 K trajectory. Local dipole moment (red arrow) that the isotropic Cs<sup>+</sup> produces due to its preferential localization in either of two off-center sites of the cavity.

Given that CsPbBr<sub>3</sub> adopts an orthorhombic structure at temperatures lower than 361 K, we expect the Pb–Br–Pb angle distribution to be represented by angles that deviate from 180°. This is indeed the case for temperatures less than 150 K, where the angle distributions have symmetric Gaussian forms, as shown in Figure 3A. However, for temperatures higher than 200 K the angle distributions are getting asymmetric. Especially at 300 K the percentage of Pb–Br–Pb angles around 180° is starting to get significant, consistent with the formation of pseudotetragonal domains within the orthorhombic crystal structure of CsPbBr<sub>3</sub>.

To quantify the amount of pseudotetragonal domains formed in the lattice as a function of temperature, we consider the fraction of Pb–Br–Pb angles that lie in the range of [160°, 180°]. In Figure 3B, we plot the fraction of pseudotetragonal domains defined in this way as a function of temperature. As expected, the fraction of tetragonal-like arrangements increases with temperature from 0.1 to 0.34 between 50 and 300 K. The adoption of tetragonal-like arrangements with increasing temperature does not correspond to a phase transition to the tetragonal structure since on average the phase that CsPbBr<sub>3</sub> adopts is still orthorhombic. This phenomenon can be explained by the existence of a double-well potential in which the Cs<sup>+</sup> moves. On the top of the barrier of this double-well potential, the Cs<sup>+</sup> occupies the central position between the octahedra leading to local structures with tetragonal-like arrangements that start to be populated at higher temperatures. At lower temperatures ( $k_B T \ll$  barrier height), the Cs<sup>+</sup> occupies either of two off-center sites that corresponds to the two minima of the double well.

To support these arguments, we also analyzed the Cs–Pb distance distribution shown in Figure 3C. At low temperatures, the distribution of the nearest-neighbor Cs–Pb distance is characterized by two distinct peaks. However, with increasing temperature the second peak starts to vanish leading finally at 300 K to a (slightly asymmetric) unimodal Cs–Pb distance distribution consistent with configurations in which the Cs<sup>+</sup>

occupies a position near the center of the interoctahedral cavities.

Given the temperature-dependent change in the localization of Cs<sup>+</sup>, we assumed that a local electric field produced by local dipoles (Stark-like effect) is responsible for the asymmetric PL spectra at low temperatures. For this reason, we calculated the local dipole moment among the Cs<sup>+</sup> and the center of the cavities. Figure 4A shows that, at 300 K, where Cs<sup>+</sup> assumes positions more and more near the center of the cavity, the local dipole moment is as expected zero. However, at lower temperatures, such as at 50 K (Figure 4B) the preferential localization of Cs<sup>+</sup> in either of two off-center sites in the empty space between the octahedra leads to an average local dipole moment on the order of 2.7 D quite comparable to and even higher than the permanent dipole moment of MA<sup>+</sup> of 2.2 D.<sup>32</sup> This establishes the fact that the change in the localization of Cs<sup>+</sup> shifts the PL spectra from an asymmetric form at low temperatures to a symmetric one at higher temperatures via a Stark-like effect.

The PL spectra of CsPbBr<sub>3</sub> were recorded over a temperature range of 15–300 K, and the low-temperature (<180 K) bands show a pronounced asymmetry that is lost with an increasing temperature. Similarly, the measured band gap exhibits a change of slope at ~120–150 K. Using first-principles MD simulations, we were able to identify the molecular origin of these effects by examining the structural characteristics of CsPbBr<sub>3</sub> at low and high temperatures, respectively. We conclude that the origin of the gradual disappearance of the asymmetry in the PL spectra with increasing temperature lies in the presence of a local dipole moment (i.e., Stark effect) that the isotropic Cs<sup>+</sup> produces when displaced away from the center of the cavity, due to a preferential localization in either of two off-center sites in the empty space between the octahedra at low temperatures. At higher temperatures this effect vanishes, and Cs<sup>+</sup> assumes positions more and more near the center of the cavities leading to an increment of tetragonal-like arrangements within the orthorhombic phase of CsPbBr<sub>3</sub> similar to what has been

reported in the case of MA<sup>+</sup>-based systems.<sup>24</sup> The population of these pseudotetragonal domains is not correlated with a phase transition from the orthorhombic to tetragonal phase, since the average structure of all the local structures that contain these pseudotetragonal arrangements still maintains the orthorhombic phase of CsPbBr<sub>3</sub>. Overall, our in-depth study presents intriguing results about the band-gap modulation and emission properties of CsPbBr<sub>3</sub>, a compound that has important applications in photoelectronic devices such as photodetectors, LEDs, and photovoltaic cells.

## ■ ASSOCIATED CONTENT

### Supporting Information

The Supporting Information is available free of charge at <https://pubs.acs.org/doi/10.1021/acs.jpcllett.1c00263>.

Computational and experimental details (PDF)

## ■ AUTHOR INFORMATION

### Corresponding Author

**Ursula Rothlisberger** – Laboratory of Computational Chemistry and Biochemistry, Institute of Chemical Sciences and Engineering, Ecole Polytechnique Fédérale de Lausanne, CH-1015 Lausanne, Switzerland; [orcid.org/0000-0002-1704-8591](https://orcid.org/0000-0002-1704-8591); Email: [ursula.rothlisberger@epfl.ch](mailto:ursula.rothlisberger@epfl.ch)

### Authors

**Ariadni Boziki** – Laboratory of Computational Chemistry and Biochemistry, Institute of Chemical Sciences and Engineering, Ecole Polytechnique Fédérale de Lausanne, CH-1015 Lausanne, Switzerland; [orcid.org/0000-0002-2347-8993](https://orcid.org/0000-0002-2347-8993)

**M. Ibrahim Dar** – Laboratory of Photonics and Interfaces, Institute of Chemical Sciences and Engineering, Ecole Polytechnique Fédérale de Lausanne, CH-1015 Lausanne, Switzerland; [orcid.org/0000-0001-9489-8365](https://orcid.org/0000-0001-9489-8365)

**Gwénolé Jacopin** – Laboratory of Quantum Optoelectronics, Institute of Physics, Ecole Polytechnique Fédérale de Lausanne, CH-1015 Lausanne, Switzerland

**Michael Grätzel** – Laboratory of Photonics and Interfaces, Institute of Chemical Sciences and Engineering, Ecole Polytechnique Fédérale de Lausanne, CH-1015 Lausanne, Switzerland; [orcid.org/0000-0002-0068-0195](https://orcid.org/0000-0002-0068-0195)

Complete contact information is available at:

<https://pubs.acs.org/doi/10.1021/acs.jpcllett.1c00263>

### Notes

The authors declare no competing financial interest.

## ■ ACKNOWLEDGMENTS

U.R. gratefully acknowledges funding from the Swiss National Science Foundation via individual grant No. 200020-185092, the NCCR MUST, and the Sinergia grant EPISODE. M.I.D. acknowledges funding from a Royal Society University Research Fellowship. The authors thank the Swiss National Supercomputing Centre for the computer time.

## ■ REFERENCES

- (1) Kojima, A.; Teshima, K.; Shirai, Y.; Miyasaka, T. Organometal Halide Perovskites as Visible-Light Sensitizers for Photovoltaic Cells. *J. Am. Chem. Soc.* **2009**, *131*, 6050–6051.
- (2) Akin, S.; Arora, N.; Zakeeruddin, S. M.; Grätzel, M.; Friend, R. H.; Dar, M. I. New Strategies for Defect Passivation in High-Efficiency Perovskite Solar Cells. *Adv. Energy Mater.* **2020**, *10*, 1903090.

- (3) Kim, H.-S.; Lee, C.-R.; Im, J.-H.; Lee, K.-B.; Moehl, T.; Marchioro, A.; Moon, S.-J.; Humphry-Baker, R.; Yum, J.-H.; Moser, J. E.; et al. Lead Iodide Perovskite Sensitized All-Solid-State Submicron Thin Film Mesoscopic Solar Cell with Efficiency Exceeding 9%. *Sci. Rep.* **2012**, *2*, 591.

- (4) Arora, N.; Dar, M. I.; Akin, S.; Uchida, R.; Baumeler, T.; Liu, Y.; Zakeeruddin, S. M.; Grätzel, M. Low-Cost and Highly Efficient Carbon-Based Perovskite Solar Cells Exhibiting Excellent Long-Term Operational and UV Stability. *Small* **2019**, *15*, 1904746.

- (5) Tan, Z.-K.; Moghaddam, R. S.; Lai, M. L.; Docampo, P.; Higler, R.; Deschler, F.; Price, M.; Sadhanala, A.; Pazos, L. M.; Credgington, D.; et al. Bright Light-Emitting Diodes Based on Organometal Halide Perovskite. *Nat. Nanotechnol.* **2014**, *9*, 687–692.

- (6) Yantara, N.; Bhaumik, S.; Yan, F.; Sabba, D.; Dewi, H. A.; Mathews, N.; Boix, P. P.; Demir, H. V.; Mhaisalkar, S. Inorganic Halide Perovskites for Efficient Light-Emitting Diodes. *J. Phys. Chem. Lett.* **2015**, *6*, 4360–4364.

- (7) Zhu, H.; Fu, Y.; Meng, F.; Wu, X.; Gong, Z.; Ding, Q.; Gustafsson, M. V.; Trinh, M. T.; Jin, S.; Zhu, X.-Y. Lead Halide Perovskite Nanowire Lasers with Low Lasing Thresholds and High Quality Factors. *Nat. Mater.* **2015**, *14*, 636–642.

- (8) Xu, Y.; Chen, Q.; Zhang, C.; Wang, R.; Wu, H.; Zhang, X.; Xing, G.; Yu, W. W.; Wang, X.; Zhang, Y.; et al. Two-Photon-Pumped Perovskite Semiconductor Nanocrystal Lasers. *J. Am. Chem. Soc.* **2016**, *138*, 3761–3768.

- (9) Gu, C.; Lee, J.-S. Flexible Hybrid Organic–Inorganic Perovskite Memory. *ACS Nano* **2016**, *10*, 5413–5418.

- (10) Muthu, C.; Agarwal, S.; Vijayan, A.; Hazra, P.; Jinesh, K. B.; Nair, V. C. Hybrid Perovskite Nanoparticles for High-Performance Resistive Random Access Memory Devices: Control of Operational Parameters through Chloride Doping. *Adv. Mater. Interfaces* **2016**, *3*, 1600092.

- (11) Yakunin, S.; Sytnyk, M.; Kriegner, D.; Shrestha, S.; Richter, M.; Matt, G. J.; Azimi, H.; Brabec, C. J.; Stangl, J.; Kovalenko, M. V.; et al. Detection of X-ray Photons by Solution-Processed Lead Halide Perovskites. *Nat. Photonics* **2015**, *9*, 444–449.

- (12) Wei, H.; Fang, Y.; Mulligan, P.; Chuirazzi, W.; Fang, H.-H.; Wang, C.; Ecker, B. R.; Gao, Y.; Loi, M. A.; Cao, L.; et al. Sensitive X-ray Detectors Made of Methylammonium Lead Tribromide Perovskite Single Crystals. *Nat. Photonics* **2016**, *10*, 333–339.

- (13) Kim, Y.-J.; Dang, T.-V.; Choi, H.-J.; Park, B.-J.; Eom, J.-H.; Song, H.-A.; Seol, D.; Kim, Y.; Shin, S.-H.; Nah, J.; et al. Piezoelectric Properties of CH<sub>3</sub>NH<sub>3</sub>PbI<sub>3</sub> Perovskite Thin Films and their Applications in Piezoelectric Generators. *J. Mater. Chem. A* **2016**, *4*, 756–763.

- (14) Eaton, S. W.; Lai, M.; Gibson, N. A.; Wong, A. B.; Dou, L.; Ma, J.; Wang, L.-W.; Leone, S. R.; Yang, P. Lasing in Robust Cesium Lead Halide Perovskite Nanowires. *Proc. Natl. Acad. Sci. U. S. A.* **2016**, *113*, 1993.

- (15) Liu, Z.; Shang, Q.; Li, C.; Zhao, L.; Gao, Y.; Li, Q.; Chen, J.; Zhang, S.; Liu, X.; Fu, Y.; et al. Temperature-Dependent Photoluminescence and Lasing Properties of CsPbBr<sub>3</sub> Nanowires. *Appl. Phys. Lett.* **2019**, *114*, 101902.

- (16) Stoumpos, C. C.; Malliakas, C. D.; Peters, J. A.; Liu, Z.; Sebastian, M.; Im, J.; Chasapis, T. C.; Wibowo, A. C.; Chung, D. Y.; Freeman, A. J.; et al. Crystal Growth of the Perovskite Semiconductor CsPbBr<sub>3</sub>: A New Material for High-Energy Radiation Detection. *Cryst. Growth Des.* **2013**, *13*, 2722–2727.

- (17) Du, X.; Wu, G.; Cheng, J.; Dang, H.; Ma, K.; Zhang, Y.-W.; Tan, P.-F.; Chen, S. High-Quality CsPbBr<sub>3</sub> Perovskite Nanocrystals for Quantum Dot Light-Emitting Diodes. *RSC Adv.* **2017**, *7*, 10391–10396.

- (18) Yang, D.; Li, P.; Zou, Y.; Cao, M.; Hu, H.; Zhong, Q.; Hu, J.; Sun, B.; Duhm, S.; Xu, Y.; Zhang, Q. Interfacial Synthesis of Monodisperse CsPbBr<sub>3</sub> Nanorods with Tunable Aspect Ratio and Clean Surface for Efficient Light-Emitting Diode Applications. *Chem. Mater.* **2019**, *31*, 1575–1583.

- (19) Wu, K.; Liang, G.; Shang, Q.; Ren, Y.; Kong, D.; Lian, T. Ultrafast Interfacial Electron and Hole Transfer from CsPbBr<sub>3</sub>

Perovskite Quantum Dots. *J. Am. Chem. Soc.* **2015**, *137*, 12792–12795.

(20) Xue, J.; Yang, D.; Cai, B.; Xu, X.; Wang, J.; Ma, H.; Yu, X.; Yuan, G.; Zou, Y.; Song, J.; Zeng, H. Photon-Induced Reversible Phase Transition in CsPbBr<sub>3</sub> Perovskite. *Adv. Funct. Mater.* **2019**, *29*, 1807922.

(21) Möller, C. H. R. K. N. Crystal Structure and Photoconductivity of Cesium Plumbohalides. *Nature* **1958**, *182*, 1436.

(22) Hirotsu, S.; Harada, J.; Iizumi, M.; Gesi, K. Structural Phase Transitions in CsPbBr<sub>3</sub>. *J. Phys. Soc. Jpn.* **1974**, *37*, 1393–1398.

(23) Trots, D. M.; Myagkota, S. V. High-Temperature Structural Evolution of Caesium and Rubidium Triiodoplumbates. *J. Phys. Chem. Solids* **2008**, *69*, 2520–2526.

(24) Dar, M. I.; Jacopin, G.; Meloni, S.; Mattoni, A.; Arora, N.; Boziki, A.; Zakeeruddin, S. M.; Rothlisberger, U.; Grätzel, M. Origin of Unusual Bandgap Shift and Dual Emission in Organic-Inorganic Lead Halide Perovskites. *Sci. Adv.* **2016**, *2*, No. e1601156.

(25) Wright, A. D.; Verdi, C.; Milot, R. L.; Eperon, G. E.; Pérez-Osorio, M. A.; Snaith, H. J.; Giustino, F.; Johnston, M. B.; Herz, L. M. Electron–Phonon Coupling in Hybrid Lead Halide Perovskites. *Nat. Commun.* **2016**, *7*, 11755.

(26) Fang, H.-H.; Raissa, R.; Abdu-Aguye, M.; Adjokatse, S.; Blake, G. R.; Even, J.; Loi, M. A. Photophysics of Organic–Inorganic Hybrid Lead Iodide Perovskite Single Crystals. *Adv. Funct. Mater.* **2015**, *25*, 2378–2385.

(27) Han, Q.; Wu, W.; Liu, W.; Yang, Q.; Yang, Y. Temperature-Dependent Photoluminescence of CsPbX<sub>3</sub> Nanocrystal Films. *J. Lumin.* **2018**, *198*, 350–356.

(28) Dey, A.; Rathod, P.; Kabra, D. Role of Localized States in Photoluminescence Dynamics of High Optical Gain CsPbBr<sub>3</sub> Nanocrystals. *Adv. Opt. Mater.* **2018**, *6*, 1800109.

(29) Lee, S. M.; Moon, C. J.; Lim, H.; Lee, Y.; Choi, M. Y.; Bang, J. Temperature-Dependent Photoluminescence of Cesium Lead Halide Perovskite Quantum Dots: Splitting of the Photoluminescence Peaks of CsPbBr<sub>3</sub> and CsPb(Br/I)<sub>3</sub> Quantum Dots at Low Temperature. *J. Phys. Chem. C* **2017**, *121*, 26054–26062.

(30) Car, R.; Parrinello, M. Unified Approach for Molecular Dynamics and Density-Functional Theory. *Phys. Rev. Lett.* **1985**, *55*, 2471–2474.

(31) Yadav, P.; Alotaibi, M. H.; Arora, N.; Dar, M. I.; Zakeeruddin, S. M.; Grätzel, M. Influence of the Nature of A Cation on Dynamics of Charge Transfer Processes in Perovskite Solar Cells. *Adv. Funct. Mater.* **2018**, *28*, 1706073.

(32) Zheng, F.; Takenaka, H.; Wang, F.; Koocher, N. Z.; Rappe, A. M. First-Principles Calculation of the Bulk Photovoltaic Effect in CH<sub>3</sub>NH<sub>3</sub>PbI<sub>3</sub> and CH<sub>3</sub>NH<sub>3</sub>PbI<sub>3</sub>–xCl<sub>x</sub>. *J. Phys. Chem. Lett.* **2015**, *6*, 31–37.